JOURNAL OF MAGNETIC RESONANCE IMAGING 35:1274–1289 (2012)

Review: MR Physics for Clinicians

Gradient Echo Imaging

CME

Michael Markl, PhD,[1,2]* and Jochen Leupold, PhD[3]

This article is accredited as a journal-based CME activity. If you wish to receive credit for this activity, please refer to the website: www.wileyhealthylearning.com

ACCREDITATION AND DESIGNATION STATEMENT

Blackwell Futura Media Services designates this journal-based CME activity for a maximum of 1 *AMA PRA Category 1 Credit*™. Physicians should only claim credit commensurate with the extent of their participation in the activity.

Blackwell Futura Media Services is accredited by the Accreditation Council for Continuing Medical Education to provide continuing medical education for physicians.

EDUCATIONAL OBJECTIVES

Upon completion of this educational activity, participants will be better able to evaluate the effectiveness of spin echo imaging in comparison to the basic principles of gradient echo formation.

ACTIVITY DISCLOSURES

No commercial support has been accepted related to the development or publication of this activity.

Faculty Disclosures:

The following contributors have no conflicts of interest to disclose:

Editor-in-Chief: C. Leon Partain, MD, PhD

CME Editor: Scott B. Reeder, MD, PhD

CME Committee: Scott Nagle, MD, PhD, Pratik Mukherjee, MD, PhD, Shreyas Vasanawala, MD, PhD, Bonnie Joe, MD, PhD, Tim Leiner, MD, PhD, Sabine Weckbach, MD, Frank Korosec, PhD

Authors: Michael Markl, PhD, Jochen Leupold, PhD

This manuscript underwent peer review in line with the standards of editorial integrity and publication ethics maintained by *Journal of Magnetic Resonance Imaging*. The peer reviewers have no relevant financial relationships. The peer review process for *Journal of Magnetic Resonance Imaging* is double-blinded. As such, the identities of the reviewers are not disclosed in line with the standard accepted practices of medical journal peer review.

Conflicts of interest have been identified and resolved in accordance with Blackwell Futura Media Services's Policy on Activity Disclosure and Conflict of Interest. No relevant financial relationships exist for any individual in control of the content and therefore there were no conflicts to resolve.

INSTRUCTIONS ON RECEIVING CREDIT

For information on applicability and acceptance of CME credit for this activity, please consult your professional licensing board.

This activity is designed to be completed within an hour; physicians should claim only those credits that reflect the time actually spent in the activity. To successfully earn credit, participants must complete the activity during the valid credit period.

Follow these steps to earn credit:

- Log on to www.wileyhealthylearning.com
- Read the target audience, educational objectives, and activity disclosures.
- Read the article in print or online format.
- Reflect on the article.
- Access the CME Exam, and choose the best answer to each question.
- Complete the required evaluation component of the activity.

This activity will be available for CME credit for twelve months following its publication date. At that time, it will be reviewed and potentially updated and extended for an additional period.

[1]Department of Radiology, Feinberg School of Medicine, Northwestern University, Chicago, Illinois, USA.
[2]Department of Biomedical Engineering, McCormick School of Engineering, Northwestern University, Evanston, Illinois, USA.
[3]Department of Radiology, Medical Physics, University Medical Center Freiburg, Freiburg, Germany.
*Address reprint requests to: M.M., Departments of Radiology and Biomedical Engineering, Northwestern University, 737 N. Michigan Ave., Ste. 1600, Chicago, IL 60611. E-mail: mmarkl@northwestern.edu
Received August 31, 2011; Accepted February 15, 2012.
DOI 10.1002/jmri.23638
View this article online at wileyonlinelibrary.com.

Magnetic resonance imaging (MRI) based on gradient echoes is used in a wide variety of imaging techniques and clinical applications. Gradient echo sequences form the basis for an essential group of imaging methods that find widespread use in clinical practice, particularly when fast imaging is important, as for example in cardiac MRI or contrast-enhanced MR angiography. However, the term "gradient echo sequence" is somewhat unspecific, as even images acquired with the most common sequences employing the gradient echo for data acquisition can significantly differ in signal, contrast, artifact behavior, and sensitivity to, eg, flow. This is due to the different use of sequence timing and basic sequence building blocks such as spoiler gradients or specific radiofrequency (RF) pulse phase patterns. In this article the basic principles of gradient echo formation compared to spin echo imaging are reviewed and the properties of gradient echo imaging in its simplest form (TR $\gg$ T_2) are described. Further, the most common three variants of fast gradient echo sequences (TR $<$ T_2), namely, unbalanced gradient echo, RF spoiled gradient echo, and balanced steady state free precession; are discussed. For each gradient echo sequence type, examples of applications exploiting the specific properties of the individual technique are presented.

Key Words: gradient echo; balanced SSFP; steady state free precession; RF-spoiling
J. Magn. Reson. Imaging 2012;35:1274–1289.

PRINCIPLES AND CONCEPTS of gradient echo (also "gradient recalled echo" [GRE]) imaging are the basis of many applications on modern magnetic resonance imaging (MRI) systems. Technically, the difference between spin echo (1–3) and gradient echo imaging is related to the pulse sequence elements that are used to generate an MR signal (Figure 1). While two radiofrequency (RF) pulses (90° and 180°) are used for spin refocusing and spin echo generation, GRE imaging is based on only a single RF pulse, typically <90°, in combination with readout gradient reversal (4–7). As a result, shorter repetition times (TR) and therefore faster imaging is feasible. Although signal formation is also more sensitive to magnetic field inhomogeneity caused by hardware-related imperfections of the main magnetic field (shim) or properties of tissue (magnetic susceptibility) (8–10), today's advanced hardware, particularly improved shim and gradient performance, permits the successful application of GRE imaging with reliable and reproducible image quality. Many GRE-based applications such as dynamic (CINE) cardiac imaging (11), MR angiography (12), assessment of tissue perfusion or viability (13–16), or body or musculoskeletal imaging (17,18) are an integral part of MR protocols used in routine clinical settings.

The purpose of this review is to provide an overview of the fundamental properties of GRE imaging and to describe the influence of the selection of imaging parameters on signal, contrast, and typical artifacts. Next to the fundamental properties of gradient echo formation and their consequences regarding signal and contrast of basic GRE imaging (TR $\gg$ T_2), the three most common fast GRE techniques (TR $<$ T_2) (19) are discussed in this review: balanced steady state free precession (bSSFP), unbalanced GRE, and RF spoiled gradient echo imaging. In addition, the effects of contrast agent, flow, magnetic susceptibility, and chemical shift are briefly reviewed and examples of the clinical application of different GRE techniques are provided. For further details, the reader may consult textbooks on MRI (20–22).

MR Spin Magnetization Dynamics

The MR signal is created by the nuclear proton spin magnetization of ^{1}H hydrogen atoms (23). Inside an MR system the strong magnetic field B_0 along the z-axis of the scanner (direction of the magnet bore) will result in the alignment of a certain fraction of the spin magnetization along the direction of B_0. As a result, a net "thermal equilibrium" magnetization M directed along B_0 is generated (Figure 2, left). The z-component of M characterizes the magnetization that is available for signal generation, which can be converted into transverse magnetization by RF excitation. The application of RF excitation with a flip angle α tips the available magnetization M toward the transverse plane by the angle α (Figure 2, mid). The

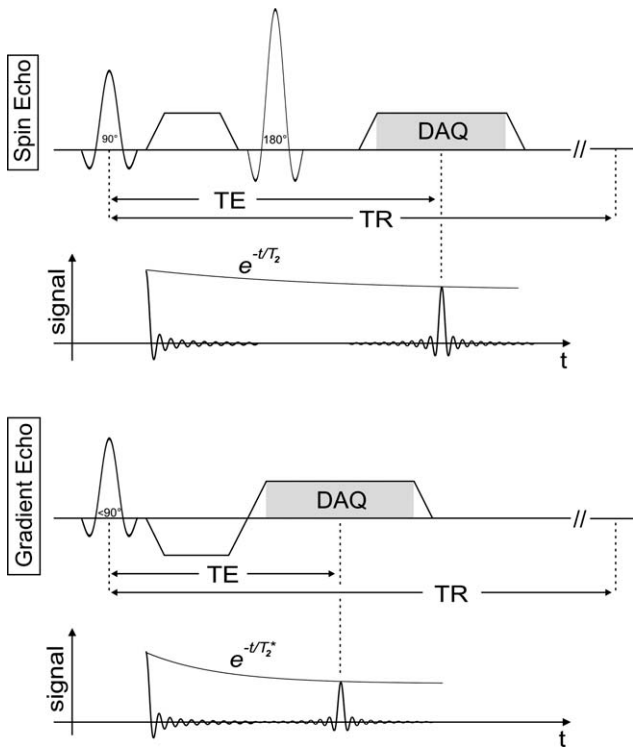

Figure 1. Simplified spin echo (top) and gradient echo (bottom) pulse sequence diagrams. The basic difference between gradient echo and spin echo imaging is related to the fact that echo formation is a result of a single RF pulse and gradient reversal while spin echo imaging uses two RF pulses, ie, a second 180° pulse, for echo generation. As a result, the gradient echo signal intensity is determined by T_2^*-decay and, contrary to the spin echo T_2-weighted signal intensity, field inhomogeneity effects are not refocused at the time of signal formation. DAQ reflects the period of data acquisition. See section Relaxation Effects for a more detailed description of T_2 and T_2^*-decay.

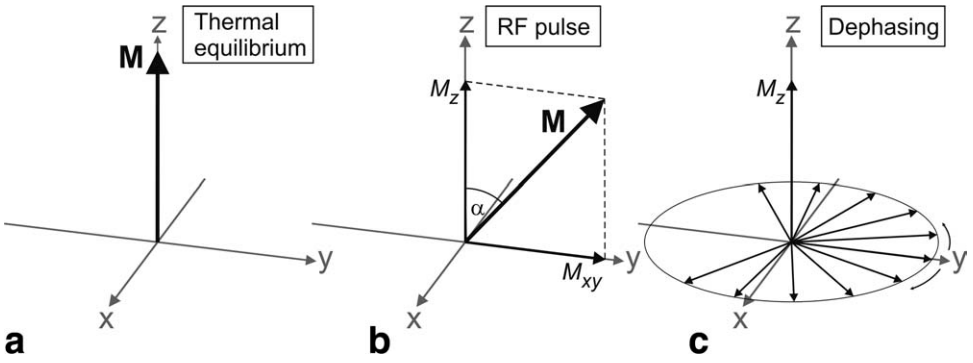

Figure 2. Spin magnetization during thermal equilibrium (**a**), after RF excitation (**b**), and following the dephasing of the transverse magnetization M_{xy} (**c**).

resulting magnetization vector can be characterized by its remaining *longitudinal* component M_z along the direction of the main magnetic field and a *transverse* component M_{xy} in the plane orthogonal to the main magnetic field B_0. Once tipped in the transverse plane, M_{xy} continuously rotates around the main magnetic field with the Larmor frequency ω_L and induces a detectable MR signal, the so-called free induction decay (FID) in a receive coil surrounding the object under investigation. The speed of the rotation of M_{xy} (precession frequency ω_L) is directly determined by the local magnetic field, ie, changes in the local magnetic field due to tissue properties (regional differences in magnetic susceptibility, eg, at air–tissue interfaces) or hardware imperfections (quality of the main magnetic field, shim) will result in locally different rotation frequencies.

Relaxation Effects

The MR signal will persist as long as M_{xy} has a nonzero component. Two different relaxation effects (T_1-recovery and T_2^*-decay) will affect the amplitude of the signal. T_1-recovery characterizes restoration of the longitudinal magnetization M_z, ie, the magnetization returns to its equilibrium magnetization M directed along B_0 by exchanging energy with its environment. Typically, T_1 relaxation values are field strength-dependent (longer T_1 times at higher fields) and can vary between ≈250 msec (fat at 1.5 T), ≈700–800 msec (brain tissue at 1.5T), ≈1200 msec (blood at 1.5 T), and up to ≈3–4 sec (cerebrospinal fluid at 1.5 T).

T_1 relaxation can thus reduce the transverse magnetization M_{xy}. More important, however, local magnetic field fluctuations and associated T_2^*-effects will result in dephasing of the transverse magnetization M_{xy} and a rapid signal decay on a much shorter time scale, within milliseconds to seconds (Figure 2, right). Based on local variations of the magnetic field due to a variety of effects (susceptibility differences at air–tissue interfaces, imperfect shim, interactions between magnetic moments of neighboring spins) the transverse magnetization M_{xy} experiences different magnetic fields locally. As a result, the transverse magnetization rotates at locally different frequencies and, in a given amount of time, magnetization at different locations acquires different amounts of rotation in the transverse plane (dephasing, Figure 3, right). The differences in amount of rotation occur on a small scale such that within each voxel of an MR image the net detectable transverse magnetization M_{xy} is reduced by this dephasing effect (the vector addition of the individual magnetization components with different amount of rotation results in a reduced net transverse magnetization which determines the detectable signal for each voxel).

The dephasing of the transverse magnetization is governed by two independent processes. The decay time T_2^* is composed of spin dephasing caused by static (time-invariant) dephasing effects (T_2'-decay) and nonconstant (time-variant) field fluctuations (T_2-decay) as described by the following relationship:

$$\frac{1}{T_2^*} = \frac{1}{T_2'} + \frac{1}{T_2} \qquad [1]$$

T_2'-decay reflects the dephasing due to temporally unchanged magnetic field inhomogeneity. These originate from, eg, local differences of the magnetic properties (described by the so-called susceptibility) of tissues, fluids, contrast agents, etc., or from hardware-related magnetic field imperfections (eg, shim). In contrast, T_2-decay is caused by stochastic and temporal varying interactions between the magnetic moments of neighboring spins. Due to the stochastic nature of this process, the dephasing effects associated with T_2-decay cannot be reversed with a spin echo sequence. In contrast, dephasing caused by deterministic T_2' can be fully time-reversed with the spin-echo.

Spin and Gradient Echo Formation

For a spin echo experiment (Figs. 1, 3, top), two RF pulses (90° and 180°) are used for echo generation. During the time between the 90° and 180° pulses, the transverse magnetization M_{xy} starts to dephase according to T_2' and T_2 effects. The second RF pulse with a flip angle of 180°, called a refocusing pulse, is used to flip over (invert) the magnetization which reverses the rotation direction of all transverse magnetization components M_{xy}. Dephasing that has occurred as result of static (T_2') effects, such as susceptibility or field imperfections (9), is reversed. This process leads to the formation of a spin echo at echo time TE when the T_2'-dephasing has effectively been nullified. Spin echo imaging thus compensates for static magnetic field effects and the signal strength is governed by the remaining T_2-induced dephasing and signal decay.

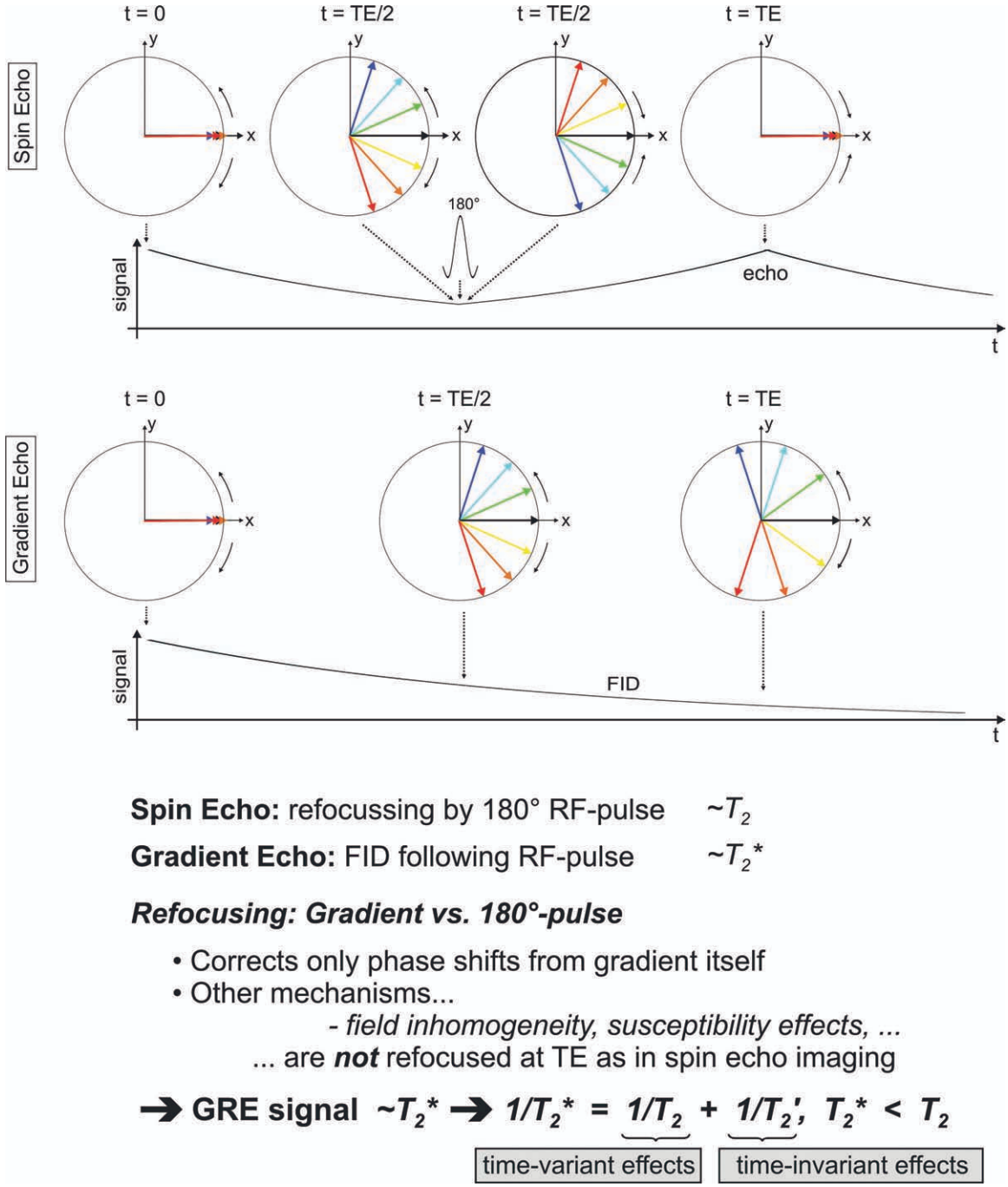

Figure 3. Signal formation for spin echo (top) and gradient echo (bottom) imaging. Top: The 180° refocusing pulse for spin echo imaging flips over magnetization and reverses the rotation direction of the transverse magnetization and results in a compensation of dephasing caused by the T_2' effect resulting in the rephasing of the magnetization at echo time TE. The colored arrows represent exemplary magnetization vectors. Bottom: For gradient echo imaging, the dephasing is not reversed. Signal and contrast are determined by both T_2' and T_2 effects. Note that shorter echo times are necessary for detectable gradient echo signal intensity.

The situation is different for GRE imaging (Figs. 1, 3, bottom), which uses a single RF pulse in combination with readout gradient reversal such that the net gradient area is zero at echo time TE. The gradient echo sequence omits the formation of a spin echo and directly uses the signal from the free induction decay following the RF excitation pulse. Mechanisms such as field inhomogeneity or susceptibility are not refocused with the gradient echo at echo time TE and will influence the signal and contrast. Note that T_2^* includes both T_2 and static T_2'-field effects (Figure 3) and is typically much shorter than T_2 alone. As a result, GRE signal intensity decays much faster and echo times have to be shorter than for spin echo imaging in order to yield sufficient signal intensity.

In short, while spin echoes are RF-refocused and provide T_2-dependent signal strength, GRE imaging is gradient refocused and has echo amplitudes determined

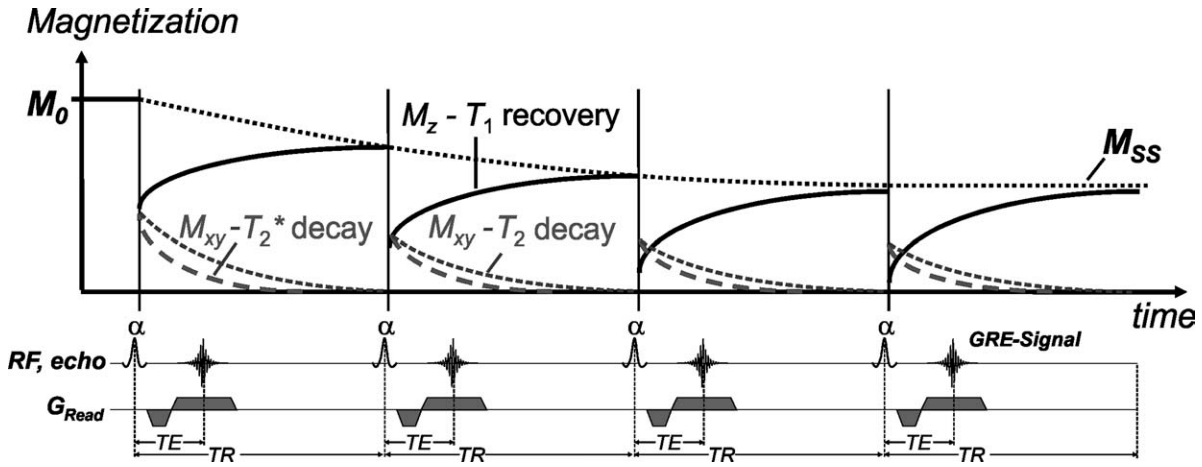

Figure 4. Steady state formation for basic GRE imaging (TR $\gg T_2$). Repeated RF excitation results in a reduction of the longitudinal magnetization (M_z) for consecutive repetition times (TR) until the steady state magnetization (M_{SS}) is reached. M_{xy} fully decays prior to each RF-excitation pulse and does not contribute to the steady state formation. The steady state magnetization (M_{SS}) which defines the signal intensity for basic GRE imaging is determined by T_1, TR, and the flip angle α.

by T_2^*-decay (Figure 3). Note that the formation of a (gradient) echo instead of a pure FID leads to better quality of the magnitude image. The symmetric shape of the echo is beneficial to the Fourier transform. Recording a pure FID (exponential decay) with a readout gradient only and without a preceding dephasing gradient would be detrimental to image quality (24).

Basic GRE Imaging (TR $\gg$ T_2)

MRI typically consists of several repetitions of a basic pulse sequence module with given repetition and echo times TR and TE until all data for a complete 2D or 3D dataset are collected, as illustrated in Figure 4. As a consequence, the timing of the acquisition, ie, TE and TR relative to signal recovery (T_1) and decay (T_2, T_2^*), will determine signal intensity and contrast. A gradient echo sequence acts as a pure progressive saturation sequence on longitudinal magnetization M_z, such that a so-called steady state will build up after several RF excitations.

To illustrate such a steady state formation, Figure 4 shows the temporal evolution of the magnetization components M_z and M_{xy} over several pulse sequence repetitions for basic GRE imaging with repetition times TR much greater than T_2. Due to the long TR, the transverse magnetization M_{xy} (dashed lines) completely decays prior to each new RF excitation. However, since TR is typically shorter than, or on the order of T_1, the longitudinal magnetization (solid lines) will not fully recover to its initial amplitude M_0. Instead, after several repetitions a new longitudinal equilibrium magnetization M_{SS} is reached, the "steady state." The signal intensity in the MR image is determined by the available longitudinal magnetization M_{SS} in the steady state that can be converted into detectable MR signal. The steady state value M_{SS} can be calculated according to the so-called "Ernst equation" (25):

$$M_{SS} = M_0 \frac{1 - e^{-TR/T_1}}{1 - e^{-TR/T_1}\cos\alpha} \qquad [2]$$

which determines the signal intensity for basic GRE imaging. Basic GRE images are thus T_1-weighted and the signal intensity is determined by the ratio TR/T_1

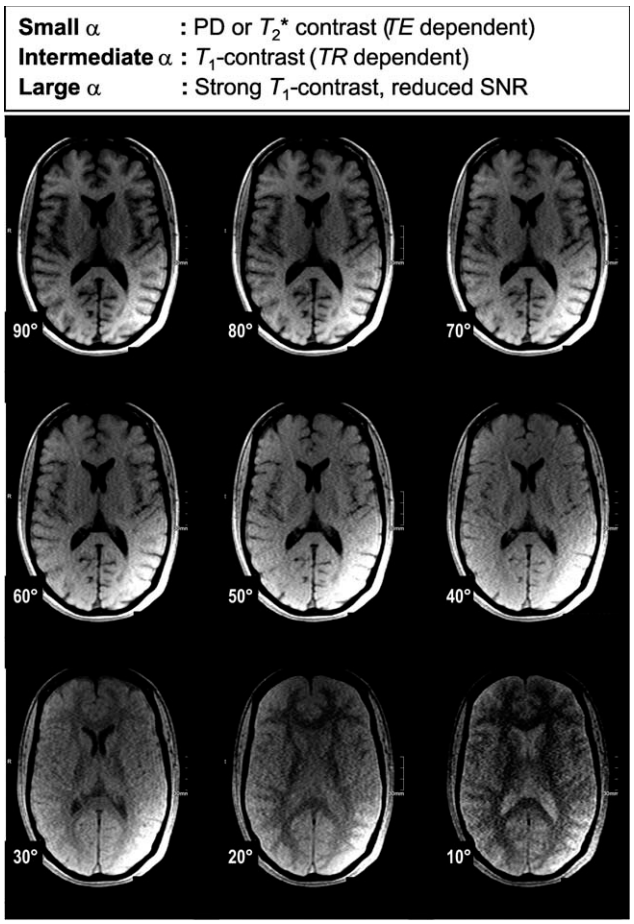

Figure 5. Cranial images acquired with basic GRE imaging (TR = 500 msec, TE = 4 msec, TR $\gg$ T_2) demonstrate signal and contrast behavior as a function of flip angle. PD, proton density.

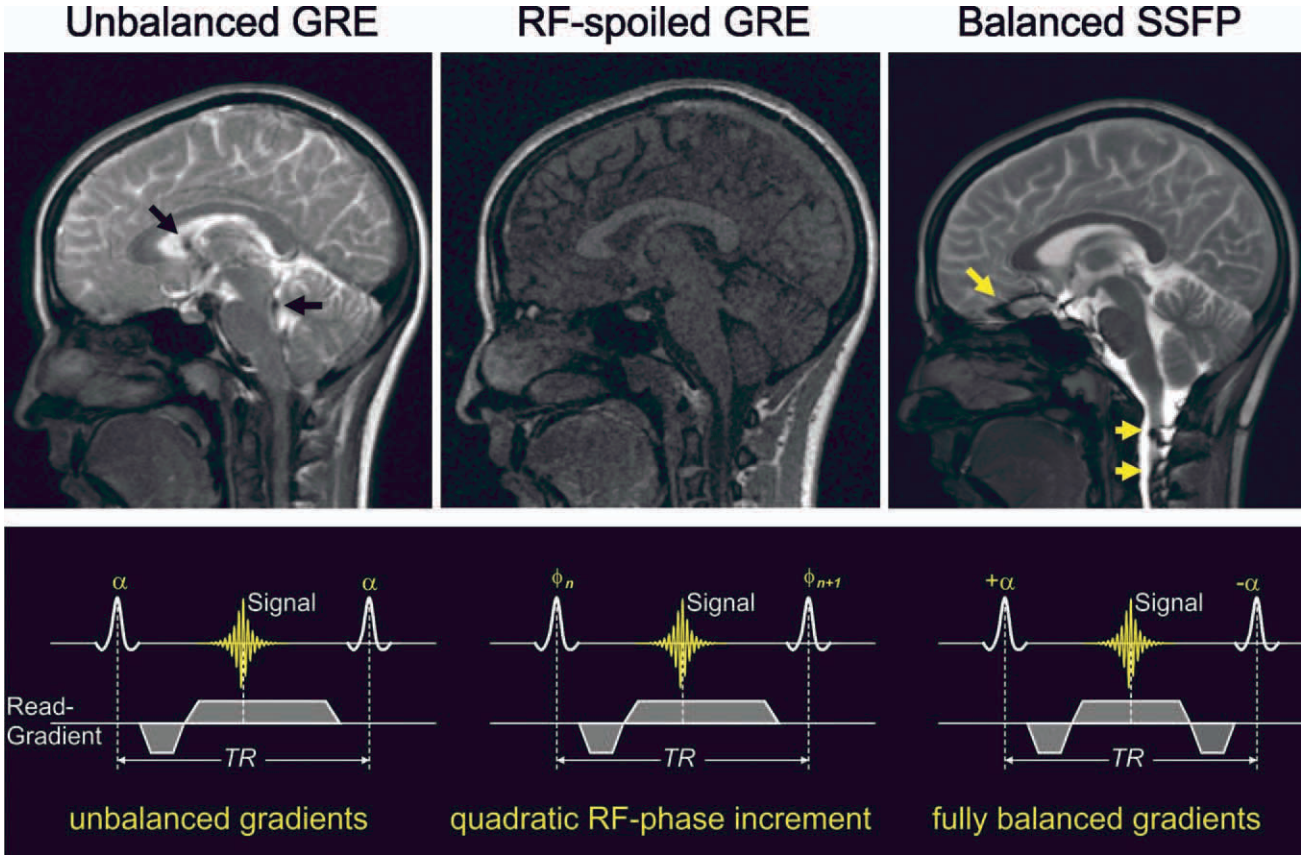

Figure 6. Comparison of the three variants of fast gradient echo (GRE) imaging. Note that all three images were acquired with short TE and TR. Unbalanced GRE (left) shows mixed T_2/T_1 contrast and cerebrospinal fluid (CSF) flow artifacts (signal void, black arrows) due to its sensitivity to flow. In addition, CSF is clearly attenuated in the spinal cannel compared to bSSFP. CSF flow acts in a similar way as RF spoiling and thus results in T_1-weighted dark CSF signal. Pure T_1 contrast can be restored in RF-spoiled GRE (mid) accompanied by a loss in SNR. Balanced SSFP (right) provides high SNR and good fluid-tissue contrast but banding artifacts (yellow arrows) demonstrate its sensitivity to local field inhomogeneity. [Color figure can be viewed in the online issue, which is available at wileyonlinelibrary.com.]

and the flip angle α. Signal intensity can be maximized for a given TR and T_1 (ie, tissue) using an optimal flip angle $\alpha = \arccos[\exp(-TR/T_1)]$, also known as the "Ernst angle." In many imaging applications, optimizing the signal from one tissue is not the major concern. More important is optimizing the contrast between two tissues (eg, lesion and healthy tissue). It should be noted that even though the signal intensities may be optimal for certain Ernst angles, contrast between tissues with different T_1 is typically maximized at higher flip angles (26,27).

The steady state formation and relationship between T_1, TR, and flip angle described above is the reason why flip angles much smaller than 90° are typically chosen for GRE imaging as compared to spin echo imaging for which maximum signal intensity is provide by 90°–180° RF pulse pairs.

Figure 5 summarizes the signal and contrast behavior for GRE imaging in the Ernst regime. Any T_2 contributions are minimized and images are predominantly T_1-weighted. The highest signal intensities are typically found at low flip angles (between 40° and 50°). Tissue contrast, however, is optimized for larger flip angles (for example, gray and white matter contrast is maximized using flip angles between 60° and 80°).

Practically, basic GRE imaging is often not very favorable because the need for a long TR leads to long acquisition times. However, the application of RF spoiling (see next section) offers the possibility of making the Ernst equation valid for short repetition times TR.

Fast GRE Imaging (TR < T_2)

Fast GRE imaging refers to the situation where TR is assumed to be short (TR $\ll$ T_1 and $<$ T_2), such that a steady state of the magnetization has built up during image acquisition (28–30). Since repetition times TR are short ($<T_2$), the transverse magnetization M_{xy} does not fully decay prior to each new RF pulse and therefore contributes to the steady state formation. In contrast to basic GRE imaging, both the longitudinal (M_z) and the transverse (M_{xy}) magnetization determine the final steady state signal intensity. As for basic GRE, signal intensities demonstrate strong flip angle dependence but also more complex contrast behavior, depending not only on T_1 TR, and but also T_2 (29). For this review, three different types of fast GRE sequences are distinguished, depending on how the transverse magnetization is used during the sequence TR, as illustrated in Figure 6.

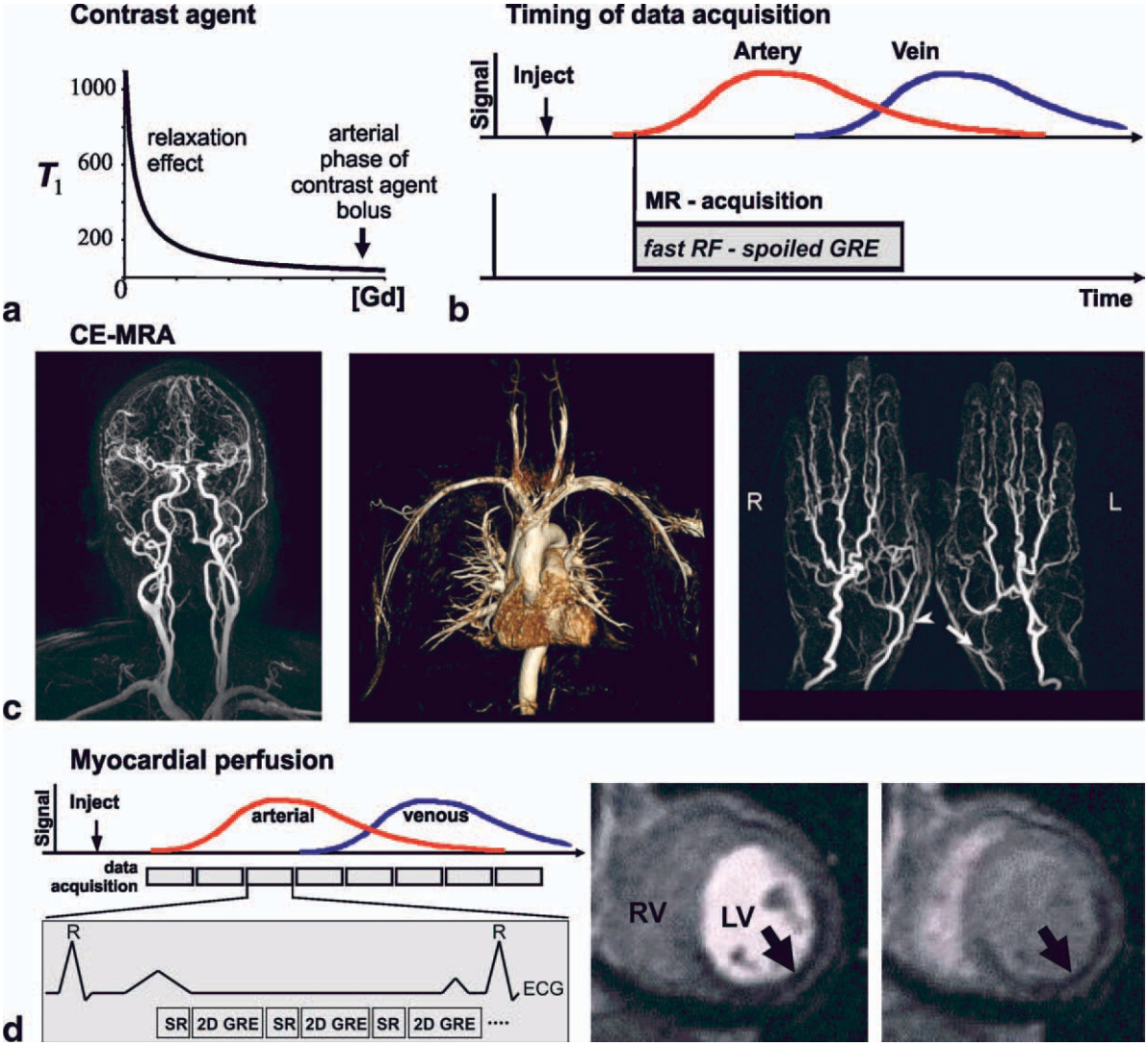

Figure 7. Contrast-enhanced (CE) MR angiography (MRA) and assessment of myocardial perfusion using fast RF-spoiled GRE imaging. **a:** Intravenous Injection of a Gd-based contrast agent results in T_1-shortening in blood during the passage of the contrast agent bolus. **b,c:** The combination of appropriate synchronization of the measurement with the arrival of the arterial contrast permits the acquisition of the contrast agent bolus passage with high arterial signal and contrast. RF-spoiled 3D GRE is ideally suited for CE-MRA due to the possibility for rapid data acquisition with pure T_1 contrast. CE-MRA can be applied in all vascular regions throughout the body as illustrated for cervical and cranial arteries (left), the thoracic aorta (mid), and hand (right). **d:** The first-pass arterial passage of contrast agent through myocardial tissue can monitored using ECG gated saturation recovery (SR) fast 2D RF spoiled GRE. In typical clinical applications, 3–5 short axis slices are acquired per RR-interval permitting the measurement of myocardial signal changes during contrast agent passage with a temporal update rate of one heartbeat. Prior to data acquisition for each slice, a 90° SR pulse is used to enhance contrast between enhancing and nonenhancing tissue. The two short axis images demonstrate an endocardial perfusion defect (arrows) during early (left) and late (right) arterial phases. [Color figure can be viewed in the online issue, which is available at wileyonlinelibrary.com.]

Unbalanced GRE

After the readout process, additional "spoiler" gradients are used to effectively average over different dephasing states of the transverse magnetization. The net gradient area is nonzero but constant within each TR.

RF Spoiled GRE

The phase of the RF pulses is systematically incremented, leading to a steady state that is approximately T_1-weighted according to the Ernst equation. As for unbalanced GRE, a spoiler gradient is necessary as well.

Balanced SSFP (bSSFP)

The gradients are arranged such that the net gradient area over one repetition time TR is zero along each axis. This results in an efficient "recycling" of all available magnetization for MR signal generation but with the undesirable result of increased sensitivity to field inhomogeneities.

A more generic name for the whole family of fast GRE sequences that is often used is "SSFP" (steady-

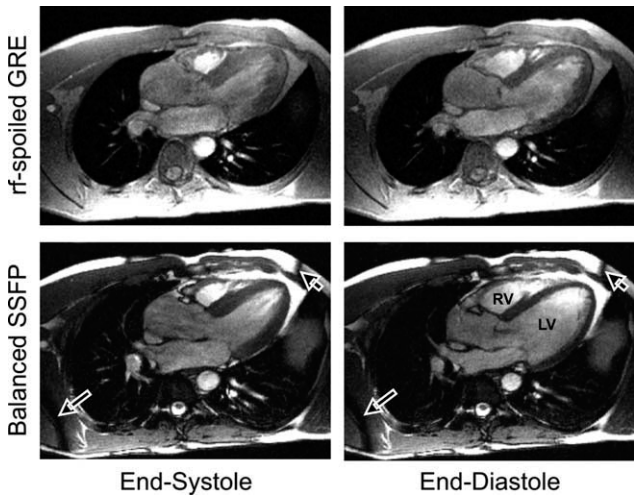

Figure 8. Time-resolved ECG-gated cardiac imaging with bSSFP and RF spoiled GRE. Improved image quality and enhanced blood–tissue contrast for bSSFP are clearly visible. Note the appearance of SSFP banding artifacts (arrows) visible as signal void in regions of increased field inhomogeneity. LV, left ventricle; RV, right ventricle.

state free precession) (31). This term refers to magnetization precessing freely (ie, without being exposed to RF) between consecutive RF excitation pulses. In this context, some confusion can result from nomenclature of these sequences, as there are different acronyms used in the literature and by different vendors for one and the same sequence. Moreover, some acronyms have changed their meaning over the years (eg, the acronym FISP (32)). The only advice that can be given is to read publications thoroughly and to not rely on the meaning of acronyms. An overview of fast GRE techniques and most common vendor-specific acronyms typically used for the different sequence types is also provided in the review article by Elster (33) and in Figure 10.

Unbalanced GRE. The simplest form of fast GRE imaging, unbalanced GRE, corresponds to the basic GRE pulse sequence with short TR ($<T_2$) and "spoiler gradients" to provide sufficient dephasing of the transverse magnetization. In the example in Figure 6 (left), spoiling is simply accomplished by lengthening the readout gradient prior to application of the next RF excitation. Despite the spoiler effect, the transverse magnetization does not fully decay before the execution of the next RF pulse such that unbalance GRE provides high signal-to-noise ratio (SNR) due to coherent use of magnetization but offers complex T_2/T_1-contrast (as opposed to pure T_1 contrast for basic GRE with TR $\gg T_2$) that may make image interpretation difficult. In addition, the complex interaction of nondecayed transverse magnetization over several TR intervals can result in flow-induced artifacts, as shown in Figure 6 (left, black arrows).

The mixed T_2/T_1-contrast and sensitivity to flow and motion artifacts are often problematic for clinical applications. As a result, unbalanced GRE does not play an important role in routine clinical applications. Nevertheless, the method represents an important basis for fast GRE imaging. To address the shortcoming of unbalanced GRE, two different fast GRE variants have been developed: RF spoiled GRE and balanced SSFP.

RF spoiled GRE. One of the key features of clinically used fast GRE has been the ability to provide well-defined T_1 contrast while maintaining high imaging speed. To enhance T_1 contrast while maintaining the short repetition times, TR, necessary for fast imaging, a solution is provided by the so-called RF spoiling technique (28,34–38). As shown in Figure 6 (mid), the method is based on quadratically incrementing the phase of the RF pulse from TR to TR, eg, resulting in a phase $\phi(n)$ of the n-th RF-pulse of $\phi(n) = n(n\text{-}1)\omega/2$, with a constant number ω. The phase of an RF pulse refers to the "tipping direction" when the magnetization is flipped from the longitudinal direction to the transverse plane and determines the orientation of the magnetization after the pulse in the transversal (x-y-) plane. It can be shown that for certain RF phase increments (eg, $\omega = 117^\circ$ or 50°) the T_2 contributions from transverse magnetization can effectively be eliminated. As a result, RF spoiled fast GRE sequences are predominantly T_1-weighted. The signal intensity in RF spoiled GRE images effectively obeys the Ernst equation in the same way as for the basic GRE sequence. Note that RF spoiling does not destroy magnetization in the strict sense. Instead, RF spoiling manipulates magnetization such that the vector addition of all transverse magnetization components results in a zero net magnetization at the end of every sequence interval.

Figure 6 shows a side-by-side comparison of RF spoiled GRE and an unbalanced GRE acquisition. It is evident that RF spoiling can successfully be used to eliminate T_2 contributions and enhance T_1 contrast while maintaining short TR. It should be noted, however, that RF spoiled GRE carries an SNR penalty since the transverse magnetization does not contribute to the total MR signal.

RF spoiled GRE sequences are a common workhorse in the clinical routine and find a wide variety of applications for which the availability of T_1-contrast in combination with short scan times is essential (eg, rapid imaging for large volumetric coverage). Important applications include tissue perfusion imaging (15,16) or infarct imaging with delayed enhancement (13,14). In cardiovascular MRI, frequently employed clinical applications include first-pass myocardial perfusion imaging and contrast-enhanced MR angiography (39), which rely on the T_1 shortening of contrast agents in combination with fast imaging to capture the passage of an intravenous bolus injection (Figure 7). Historically, RF spoiling made fast T_1-weighted imaging possible and opened the door to numerous contrast-enhanced clinical applications.

A remark on the term "gradient spoiling": Cancellation of transversal magnetization components can also be established by spoiler gradients *varying* along the slice-selection direction from TR to TR (40). However, this "gradient spoiling" technique is less robust

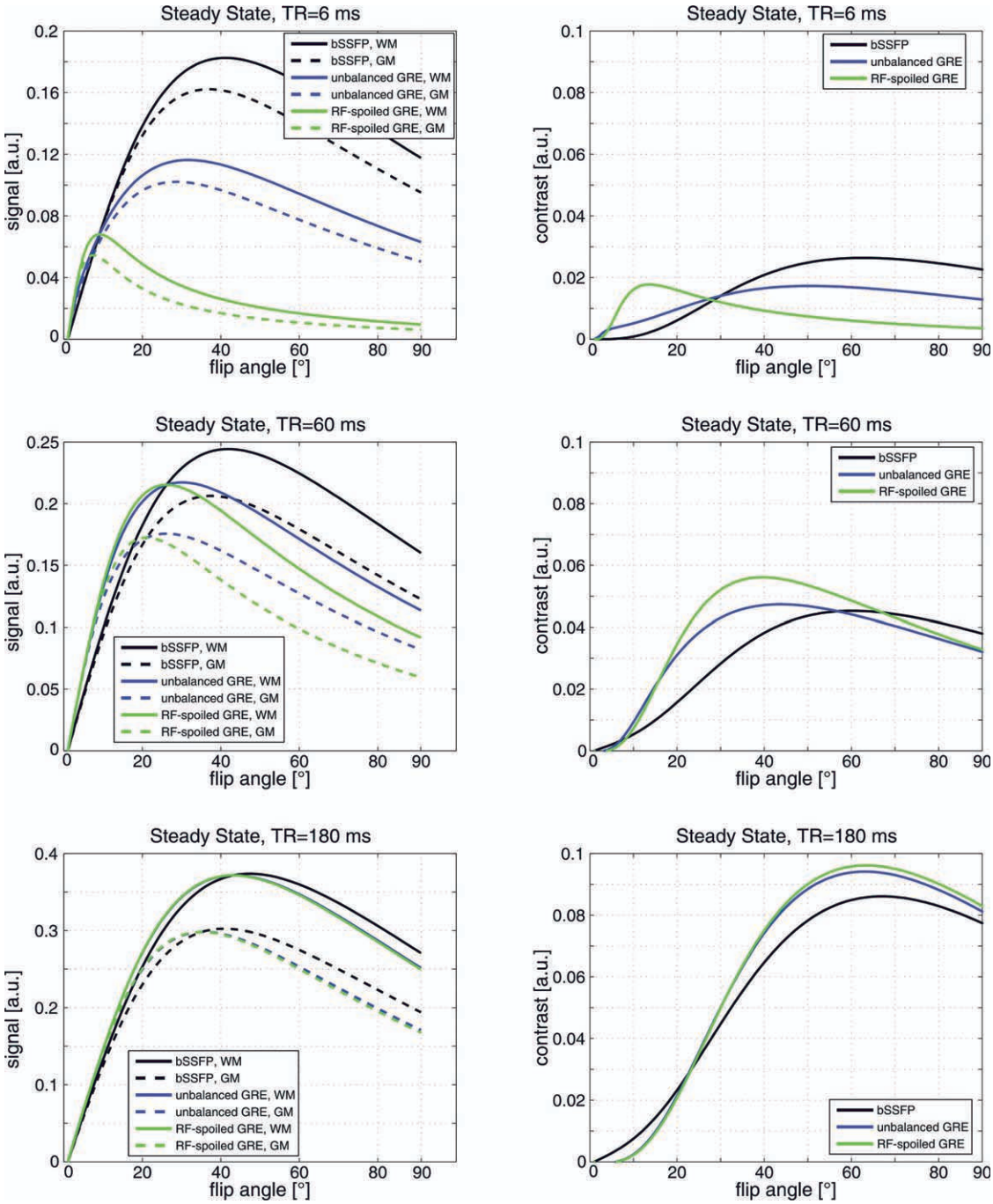

Figure 9. Simulation of signal (left column) and gray matter/white matter contrast (right column) for various GRE sequences.

than RF spoiling; therefore, it is rarely used in recent clinical GRE imaging methods (21,34). Gradient spoiling is conceptually different from the use of a *constant* spoiler gradient, which is used for both RF spoiled and unbalanced GRE. Note that in unbalanced GRE sequences, flow can also lead to T_1-weighting, as it can act in a similar way as RF spoiling (eg, attenuation of flowing CFS in Figure 6 in the spinal canal, left).

Balanced SSFP (bSSFP). A third fast GRE variant is known as bSSFP imaging (17) and has gained increased importance in a number of applications due to its superior SNR and in particular blood–tissue contrast (41,42). Compared to other GRE variants, gradients are fully balanced (ie, gradient areas sum to zero over TR, see Figure 6, right), resulting in a more efficient refocusing of the steady state magnetization and thus increased signal.

However, bSSFP also exhibits a strong sensitivity to local field offsets such as variations of the external field or regional susceptibility differences (off-resonance sensitivity) (43). Signal and contrast for bSSFP imaging are a function of the local magnetic field. If the magnetic field is nonuniform, there can be regions in the image where the signal almost completely vanishes (banding artifacts, see Figs. 6, 8).

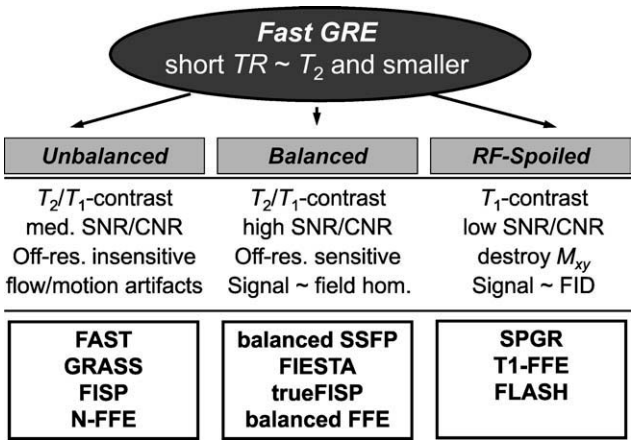

Figure 10. Fast gradient echo imaging variants, fundamental signal and contrast properties and corresponding vendor-specific acronyms.

In addition to the local field, the repetition time TR can substantially influence the spatial bSSFP signal homogeneity. As TR is increased, image quality degrades and banding artifacts in areas of high local field offsets become more and more prominent. A combination of good field homogeneity (the so-called "shim") and short repetition times is therefore crucial for artifact-free bSSFP imaging. The short repetition times needed by bSSFP can only be achieved with sufficiently fast switching and strong gradients. This is the reason why bSSFP imaging did not become widely used until the late 1990s (17), when the necessary gradient performance became available. Balanced SSFP sequences are mostly used for, but not limited to, body and cardiovascular MRI (17,42).

In addition to local field inhomogeneities, bSSFP is sensitive to any disruption of the steady state, ie, by interruption of the regularly spaced train of RF pulses. For applications that rely on repetitive magnetization preparation or added functionality, such as fat saturation, tagging preparation, or navigator gating, the steady state must be interrupted to include an appropriate preparation sequence. In order to avoid severe disruption of the steady state magnetization, the RF pulses and gradients necessary for the preparation are typically embedded into a steady state storage scheme ("$\alpha/2$ technique") as presented by Scheffler et al (44).

Both RF spoiled GRE and balance SSFP are used for dynamic cardiac imaging. If data acquisition is gated or synchronized with the cardiac RR interval, time-resolved (CINE) anatomical images can be collected to depict the dynamics of left and right ventricular function during the cardiac cycle (45). For short TR, the superior signal amplitude and improved blood-tissue contrast of bSSFP is obvious from Figure 8. However, sensitivity of bSSFP to field inhomogeneities may result in signal variations and artifacts. The effects become more prominent at higher fields (3 T and higher) such that cardiac imaging with balanced SSFP has become the method of choice at 1.5 T, while RF spoiled GRE, which is less sensitive to local field variations, is often used at 3 T. Figure 8 shows results from an

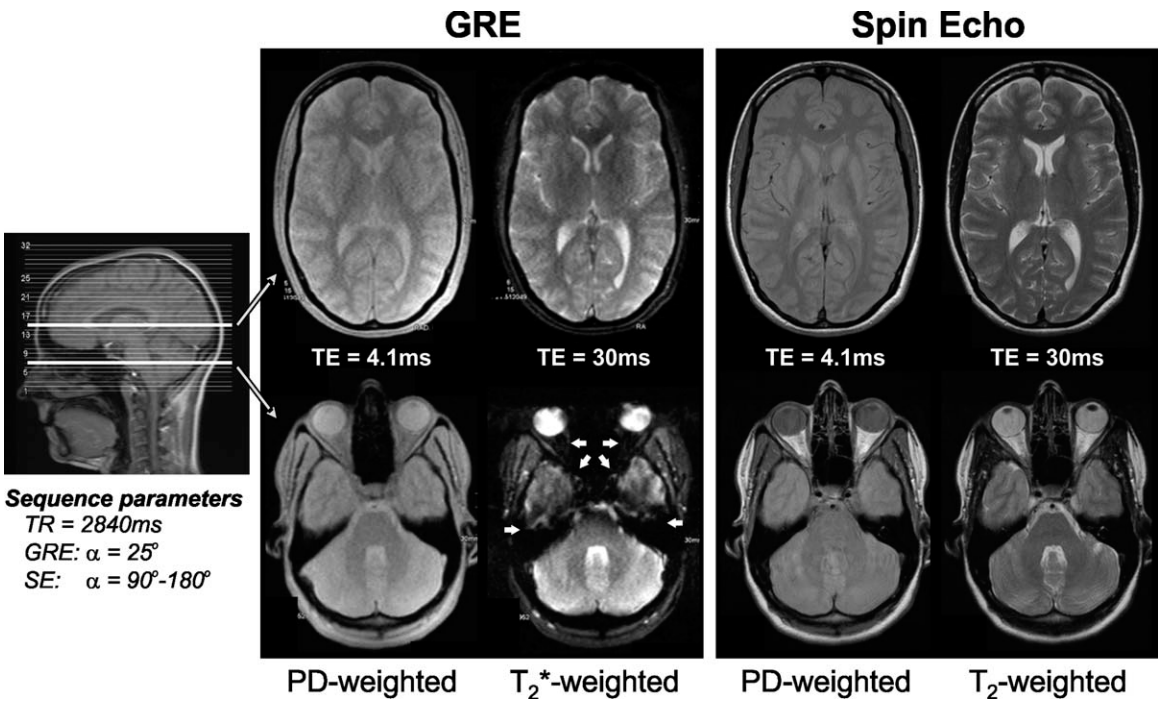

Figure 11. T_2^*-effects in GRE imaging illustrated for basic multislice 2D GRE ($TR \gg T_2$) for two images at different axial location in the head. The GRE images are compared to spin echo (SE) images at identical anatomical locations using the same echo and repetition times. For short TE = 4.1 msec, both GRE and SE images are predominantly proton density (PD)-weighted, show similar contrast, and no or only minor artifacts. Increasing echo time to TE = 30 msec, GRE images show overall signal reduction and marked signal loss in regions which have high susceptibility variations (air–tissue interfaces, white arrows). In contrast, spin echo imaging is insensitive to these effects. Note that long echo times result in T_2 contrast for SE images while GRE images are T_2^*-weighted. All images were acquired at 1.5T.

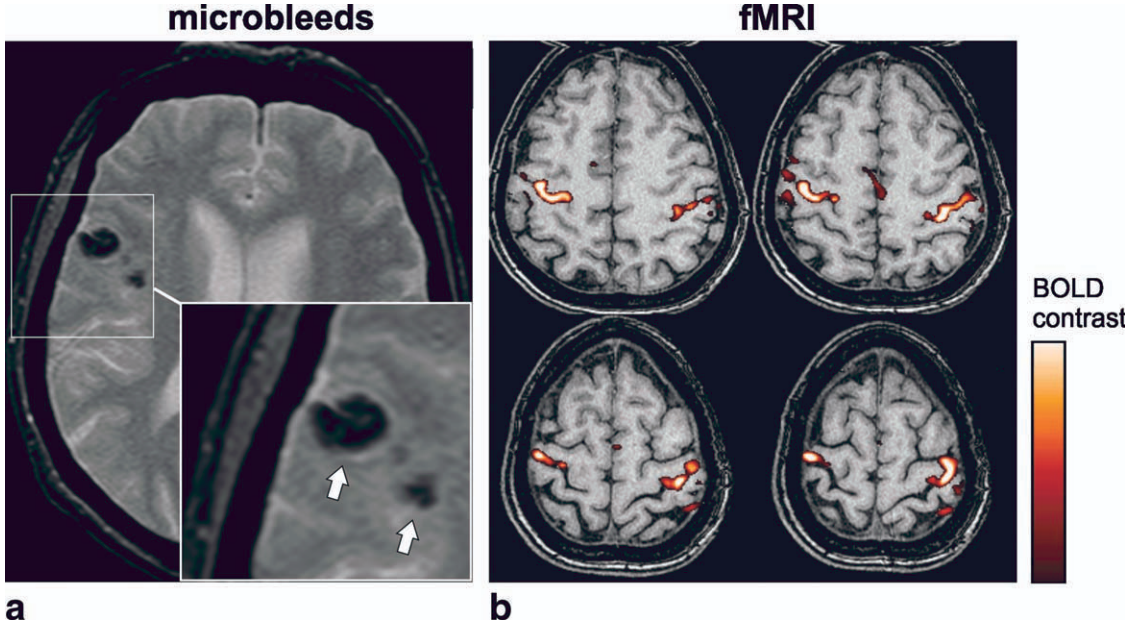

Figure 12. Examples of the application of T_2^*-weighted gradient echo imaging. **a:** Cranial 2D GRE with long echo times reveal hemosiderin deposits as a result of microbleeds (white arrows) after stroke. **b:** Functional MRI used GRE with long echo times to detect changes in regional blood T_2^* based on to changes in local blood oxygenations levels related to neuronal activity (BOLD effect).

electrocardiogram (ECG)-gated dynamic study of cardiac motion in the four-chamber view. Note the high SNR and also blood–tissue contrast of bSSFP (bottom row) as compared to RF spoiled gradient echo imaging (top row).

Comparison of Fast GRE Techniques

Figure 9 provides an overview of the signal and contrast characteristics for all three fast GRE techniques and basic GRE as a function of the flip angle used for RF excitation. Simulations based on Bloch equations have been employed to calculate signal and contrast of brain white matter (WM) and gray matter (GM). Relaxation times at 1.5 T (20) are: WM: T_1 = 600 msec, T_2 = 80 msec; and GM: T_1 = 950 msec, T_2 = 100 msec. Three different repetition times were simulated: TR = 6 msec ($\ll T_2$); TR = 60 msec ($\approx T_2$); TR = 180 msec ($>T_2$, $<T_1$). Contrast is simply the difference in signal amplitudes between WM and GM.

RF spoiled GRE shows signal behavior according to the Ernst equation, with maximum GRE signal at the Ernst angle. The maximum shifts to lower flip angles with shorter TR. Note that at the Ernst angle all three sequence variants exhibit the same signal intensity. For longer TR, the signal curves become more and more similar, with maximum signal intensity shifting closer to 90°. Contrast increases with longer TR, and is highest for RF spoiled GRE for intermediate and long TR. Simulations confirm the finding from Figure 5, contrast of RF spoiled GRE is maximized for flip angles higher than the Ernst angle (26,27).

The basic properties and commonly used acronyms of the three most widely used fast GRE techniques are summarized in Figure 10. Unbalanced GRE demonstrates high signal but rather low and complex T_2/T_1-contrast and is sensitive to flow and motion artifacts. T_1 contrast is enhanced by the application of RF spoiling but overall signal intensity is considerably reduced. Balanced SSFP imaging can offer the highest signal but suffers from strong sensitivity to local field changes and also provides mixed T_2/T_1 contrast (43).

T_2^* and Off-Resonance Effects

One of the fundamental differences between GRE and spin echo imaging is related to the fact that phase shifts from local magnetic field inhomogeneities are not refocused in GRE imaging and lead to signal decay governed by T_2^*.

In general, GRE images are thus more sensitive to artifacts due to changes in magnetic susceptibility (46). For long echo times, signal loss can be severe, as shown by the GRE images in Figure 11, where it is demonstrated that a longer TE leads to an overall decline in signal intensity and almost complete signal dropout in the frontal region with increased field inhomogeneity resulting from high susceptibility differences. For comparison, spin echo imaging is independent of these effects.

However, T_2^*-sensitivity of GRE imaging can also be beneficial and used to generate new diagnostic information, as shown in Figure 12. For example, T_2^*-contrast is used in functional MRI (fMRI) where changes in blood oxygenation that lead to alterations in T_2^* are used to analyze brain activation (Figure 12b) (47,48). Another widely used application involves the detection of bleeding in stroke patients. Microbleeds in such patients lead to local field alterations and therefore T_2^*-changes that can be visualized as signal dropouts using GRE techniques (49) with long echo times (Figure 12b). Since such bleeds are very small

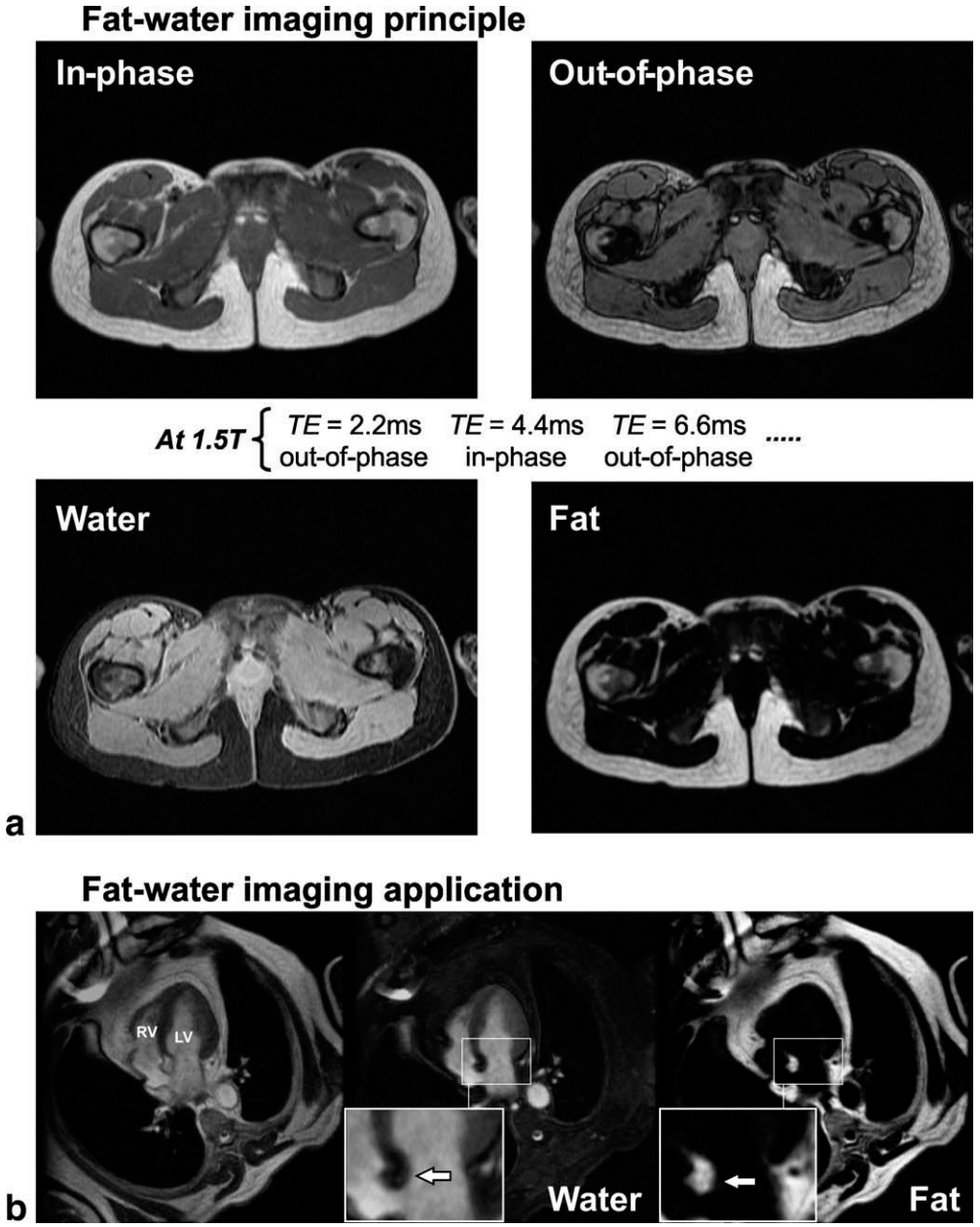

Figure 13. a: Principe of fat water imaging based on in-phase and out-of-phase images for GRE imaging with different echo times TE. Fat and water images calculated for the in-phase/out-of-phase data. **b:** Cardiac fat-water imaging in four-chamber orientation clearly showed intraarterial lipomatous signal as visible in the fat image and absent in the water image (white arrows). Fat-water imaging permitted an improved characterization of this lesion compared to standard GRE imaging (left).

and hardly detectable with any other imaging modality, T_2^*-GRE imaging is often part of the clinical routine workup of stroke patients. Furthermore, T_2^* differences are also exploited in susceptibility-weighted imaging (SWI) (50). Additional applications include the analysis of the T_2^*-dynamics in contrast agent studies (51) that can be used to generate brain perfusion maps (52,53) such as regional cerebral blood volume and flow.

A second important effect acting on the observed signal intensity of gradient echo sequences is the chemical shift. Due to the frequency difference of water and fat (220 Hz at 1.5 T, 440 Hz at 3 T), their magnetization vectors exhibit a phase difference, which depends on the echo time TE. Of special importance are the in-phase (fat and water magnetization are aligned and add) and the out-of-phase (fat and water magnetization are opposed and cancel) conditions. For a 1.5 T magnet, images can be produced that provide contrast generated by opposed (TE = 2.2 msec, 6.6 msec,...) and aligned fat and water spins (TE = 4.4 msec, 8.8 msec,...).

Figure 13a shows an example of in-phase/out-of-phase images, which can be used to analyze fat and water content in different tissues (54). Since fat and water signal add in the in-phase image, signal intensities are typically higher than in the out-of-phase images. Note the occurrence of dark rims at the

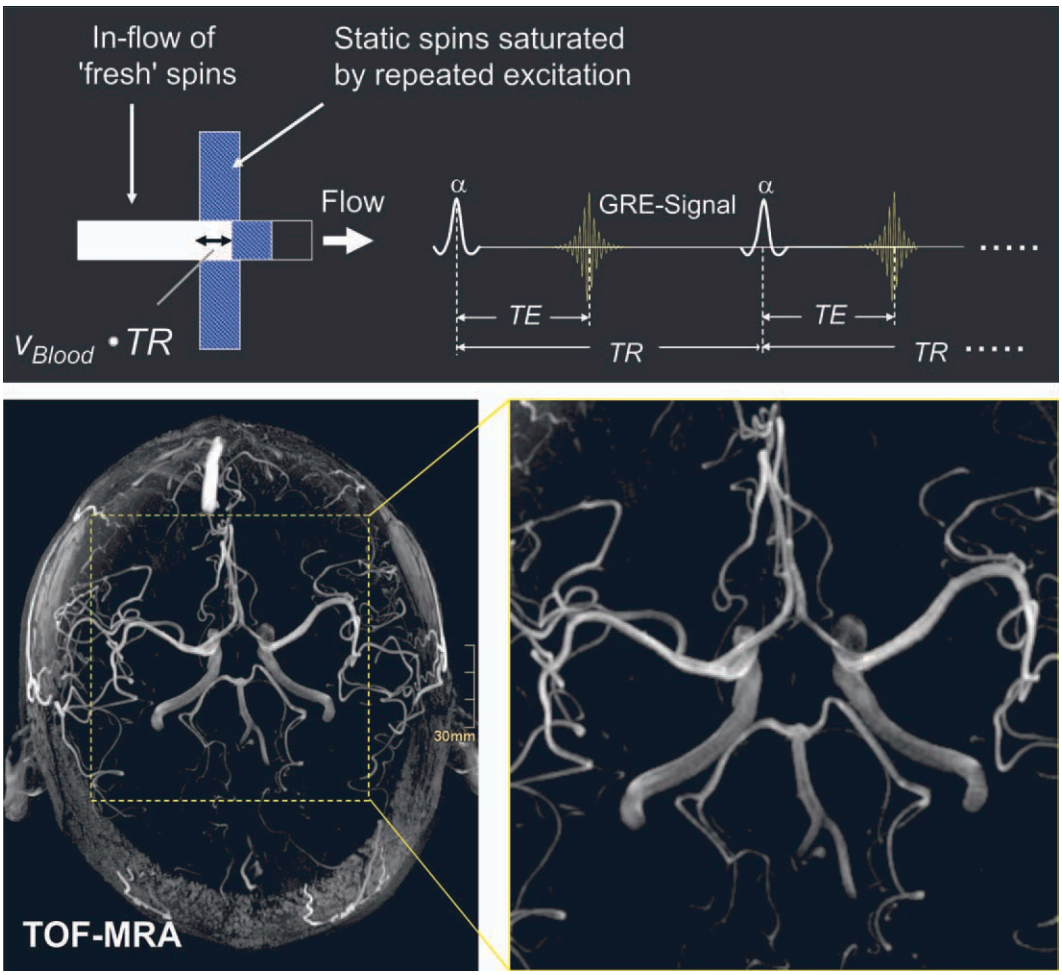

Figure 14. In-flow enhancement in GRE imaging results in bright signal of blood entering the imaging slice. In combination with saturation of static tissue this effect can be exploited to provide high blood-tissue contrast as in TOF MR angiography. [Color figure can be viewed in the online issue, which is available at wileyonlinelibrary.com.]

interface between fatty and aqueous tissues when TE is chosen to correspond to the out-of-phase condition. The signal void represents partial volume effects in pixels with roughly equal fat and water content which cancel and lead to signal void. Furthermore, the information in both images can be combined and processed for effective fat–water separation (55–57), eg, for imaging of joints for cartilage analysis (58), diagnosis of fatty liver disease (59), or lesion characterization as shown in Figure 13b.

This manifestation of the chemical shift must not be confused with the so-called "chemical shift misregistration" artifact (22), which occurs in GRE as well as in SE sequences. In this context, chemical shift can cause a spatial misregistration of fat versus water tissue depending on the bandwidth of the pulse sequence.

Flow Effects

Since signal intensity in GRE imaging is determined by repeated RF excitation, any static tissue will typically not fully recover prior to the next excitation (steady state formation), resulting in saturated and consequently reduced signal intensities. Then signal behaves according to the steady state simulations for which typical examples have been shown in Figure 9. In contrast, blood that flows into an imaging slice has not experienced a sufficient number of previous RF excitations to build up a steady state. This will lead to signal enhancement, ie, in-flow of unsaturated magnetization results in bright signal of blood as typically observed in fast GRE imaging.

Such inflow enhancement can be beneficial and used to acquire additional diagnostic information as, for example, shown in Figure 14 for time-of-flight (TOF) techniques (60,61). The in-flow enhancement is used to separate arterial or venous signal from static tissue or background signal to generate angiograms. Here the optimal flip angle for high blood/tissue contrast is usually higher than for static tissues such as the example of gray and white matter shown in Figure 5. Additionally, background (static tissue) suppression techniques such as magnetization transfer pulses can be employed (62).

In-flow can also lead to image artifacts such as misregistration and ghosting (22) that arises if laminar or

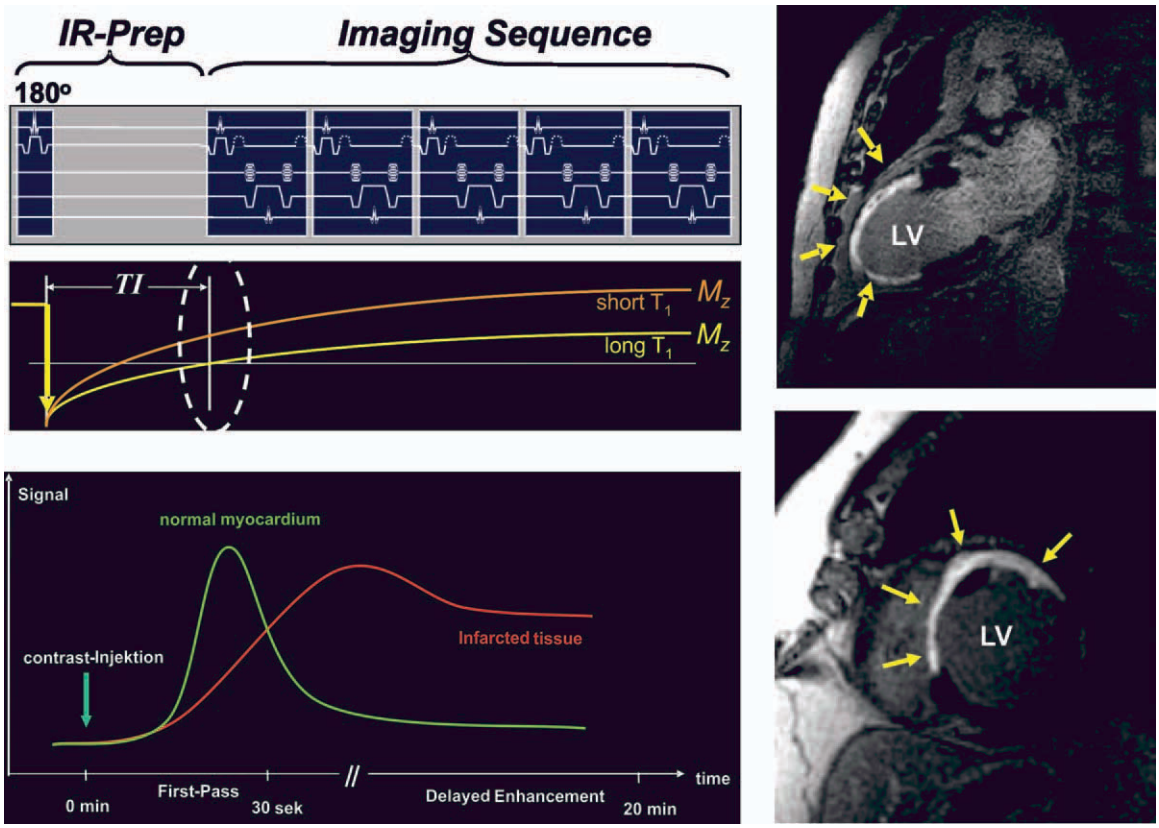

Figure 15. Left: Magnetization preparation by inversion recovery (IR) for enhanced T_1 contrast as in delayed enhancement cardiac MRI. To improve contrast between tissue with and without contrast agent uptake, the inversion time (TI) can be selected to null nonenhancing myocardial tissue (long T_1). Contrast agent that accumulates in infarcted tissue results in shorter T_1 and high GRE signal. Right: Delayed enhancement images of the left ventricle (LV) in a patient with myocardial infarction. Bright areas (arrows) mark regions with contrast agent accumulation in irreversibly damaged myocardial tissue. [Color figure can be viewed in the online issue, which is available at wileyonlinelibrary.com.]

pulsatile flow leads to amplitude or phase inconsistencies. A solution to this problems is offered by flow compensation techniques (63), which can eliminate artifacts but lead to an increase in echo and repetition times TE and TR.

Magnetization Preparation

The intrinsic contrast of GRE imaging techniques may not be sufficient, for example, when using short TRs. In this case, as can be seen from Figure 9, signal and contrast are rather poor for unbalanced and RF spoiled GRE. A potential solution is offered by magnetization preparation methods, which are used to imprint T_1 or T_2 contrast onto the longitudinal magnetization M_z and enhance the desired contrast and signal amplitude. A frequently used technique is shown in Figure 15, which illustrates enhanced T_1 weighting by inversion recovery imaging (64). Before the actual start of GRE imaging, a 180° inversion pulse is applied preceding data acquisition by the time-interval or inversion time *TI*. Depending on T_1 of the tissue and the *TI* time, certain T_1 species can be enhanced, suppressed, or even nulled. For cranial imaging, magnetization prepared rapid gradient echo (MP-RAGE) is often used clinically for anatomical imaging of the entire head with T_1-contrast. Another clinically important example of an inversion recovery application is the "delayed hyper-enhancement" technique (65), which is used to identify infarcted and nonviable tissue in patients with coronary artery disease. Here, the inversion time *TI* is selected such that the myocardial signal is nulled and only contrast agent that accumulates in infarcted tissue—and has much shorter T_1—appears bright in the GRE images (Figure 15).

DISCUSSION

In this review the basic principles of GRE imaging and the most commonly used techniques for fast GRE data acquisition have been presented. A brief summary of GRE properties is provided in Figure 16. Noticeably, the signal of a gradient echo sequence is sensitive to various T_2^*-effects, which—contrary to spin echo acquisition—are not refocused at the time of signal detection.

Signal and contrast for basic GRE imaging (TR $\gg$ T_2) depend on the formation of a steady state that is governed by the Ernst equation. T_2-contribution can be ignored, resulting in relatively simple contrast behavior depending on TR, T_1, and the flip angle. Due to the long TRs (on the order of several 100

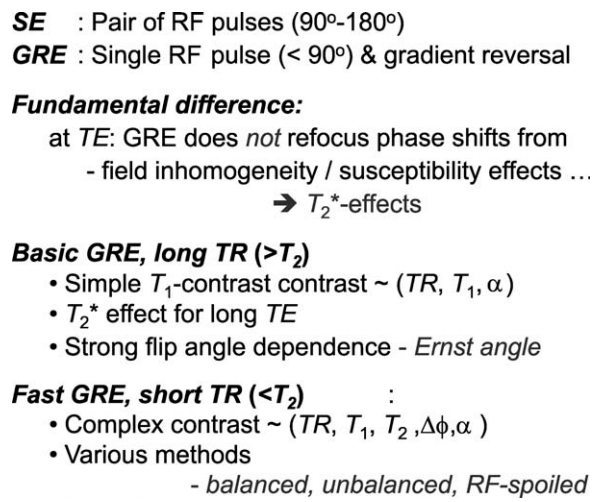

Figure 16. Summary of the properties of gradient echo imaging.

msec), basic GRE does not offer many advantages over spin echo imaging, which often provide improved image quality for similar total scan times. Basic GRE, therefore, does not play an important role in clinical applications. In contrast, fast GRE techniques provide substantially higher imaging speed and are widely used in numerous applications in the clinical routine.

Fast GRE imaging techniques (short TE and TR $\ll T_1$ and $< T_2$) demonstrate complex contrast behavior depending on TR, T_1, T_2, flip angle, and in case of bSSFP, even the local magnetic field (off-resonance effects). Unbalanced and balanced GRE techniques provide complex T_2/T_1 contrast and high SNR. Balanced SSFP offers even higher signal and especially excellent blood tissue contrast but suffers from sensitivity to local field homogeneity. T_1 contrast can be restored by the application of RF spoiling, which offers a robust and fast imaging technique for a variety of applications.

All the discussed GRE sequences rely on the principle of SSFP. It is important to note that the family of SSFP sequences contains even more members, such as PSIF (also called CE-FAST) (66,67) or echo-shifted GRE sequences (68); all of them are distinguished by the arrangement of gradient pulses. However, in clinical practice these SSFP variants play only a very minor role, and are thus not covered by this review article. The reader is referred to further literature for more information (29,35).

An important extension of GRE techniques are ultrafast GRE methods, which combine gradient echo formation with multiecho data acquisition or time-efficient sampling strategies such as spiral (69–71) or echo planar imaging (72,73). A more detailed description and discussion of the properties and methodological considerations of these techniques is beyond the scope of this article. More details can be found in a recent review article by Tsao (74).

In summary, GRE sequences play an important role in MRI due to several reasons: First, the build-up of a steady state enables fast imaging and 3D acquisitions. Second, the broad variety of contrast behavior and sensitivity to other influences such as flow makes it possible in a large number of cases to find a suitable gradient echo sequence as the matter of choice. Third, due to their robust and reliable image quality, GRE sequences can be used as acquisition modules in combination with various magnetization preparation modules.

REFERENCES

1. Hahn EL. Spin echoes. Phys Rev 1950;80:580–594.
2. Hennig J. Echoes — how to generate, recognize, use or avoid them in MR-imaging sequences. Part 2: Echoes in imaging sequences. Concepts Magn Reson 1991;3:179–192.
3. Hennig J. Echoes — how to generate, recognize, use or avoid them in MR-imaging sequences. Part 1: Fundamental and not so fundamental properties of spin echoes. Concepts Magn Reson 1991;3:125–143.
4. Edelstein WA, Hutchison JM, Johnson G, Redpath T. Spin warp NMR imaging and applications to human whole-body imaging. Phys Med Biol 1980;25:751–756.
5. Haase A, Matthaei D, Hanicke W, Frahm J. Dynamic digital subtraction imaging using fast low-angle shot MR movie sequence. Radiology 1986;160:537–541.
6. Frahm J, Haase A, Matthaei D. Rapid three-dimensional MR imaging using the FLASH technique. J Comput Assist Tomogr 1986;10:363–368.
7. Frahm J, Haase A, Matthaei D. Rapid NMR imaging of dynamic processes using the FLASH technique. Magn Reson Med 1986;3:321–327.
8. Haacke EM, Tkach JA, Parrish TB. Reduction of T2* dephasing in gradient field-echo imaging. Radiology 1989;170:457–462.
9. Posse S, Aue WP. Susceptibility artifacts in spin-echo and gradient-echo imaging. J Magn Reson 1989;88:473–492.
10. Lüdeke KM, Röschmann P, Tischler R. Susceptibility artifacts in NMR imaging. Magn Reson Imaging 1985;3:329–343.
11. Waterton JC, Jenkins JP, Zhu XP, Love HG, Isherwood I, Rowlands DJ. Magnetic resonance (MR) cine imaging of the human heart. Br J Radiol 1985;58:711–716.
12. Dumoulin CL, Hart HR Jr. Magnetic resonance angiography. Radiology 1986;161:717–720.
13. Kim RJ, Shah DJ, Judd RM. How we perform delayed enhancement imaging. J Cardiovasc Magn Reson 2003;5:505–514.
14. Kim RJ, Fieno DS, Parrish TB, et al. Relationship of MRI delayed contrast enhancement to irreversible injury, infarct age, and contractile function. Circulation 1999;100:1992–2002.
15. Sakuma H. Magnetic resonance imaging for ischemic heart disease. J Magn Reson Imaging 2007;26:3–13.
16. Schwitter J. Myocardial perfusion. J Magn Reson Imaging 2006;24:953–963.
17. Scheffler K, Lehnhardt S. Principles and applications of balanced SSFP techniques. Eur Radiol 2003;13:2409–2418.
18. Vahlensieck M, Lang P, Seelos K, Yang-Ho Sze D, Grampp S, Reiser M. Musculoskeletal MR imaging: turbo (fast) spin-echo versus conventional spin-echo and gradient-echo imaging at 0.5 Tesla. Skeletal Radiol 1994;23:607–610.
19. Sekihara K. Steady-state magnetizations in rapid NMR imaging using small flip angles and short repetition intervals. IEEE Trans Med Imaging 1987;6:157–164.
20. Haacke EM, Brown RW, Thompson MR, Venkatesan R. Magnetic resonance imaging — physical principles and sequence design. New York: John Wiley & Sons; 1999.
21. Bernstein M, King K, Zhou X. Principles of nuclear magnetic resonance in one and two dimensions. New York: Elsevier Academic Press; 2004.
22. Liang Z, Lauterbur P. Principles of magnetic resonance imaging. A signal processing perspective. New York: IEEE Press; 2000.
23. Levitt M. Spin dynamics. New York: Wiley & Sons; 2001.
24. Gadian D. NMR and its applications to living systems. Oxford: Oxford University Press; 1996.
25. Ernst R, Bodenhausen G, Wokaun A. Principles of nuclear magnetic resonance in one and two dimensions. Oxford: Clarendon Press; 1987.

26. Stadnik TW, Luypaert RR, Neirynck EC, Osteaux M. Optimization of sequence parameters in fast MR imaging of the brain with FLASH. AJNR Am J Neuroradiol 1989;10:357–362.
27. Pelc NJ. Optimization of flip angle for T1 dependent contrast in MRI. Magn Reson Med 1993;29:695–699.
28. Sobol WT, Gauntt DM. On the stationary states in gradient echo imaging. J Magn Reson Imaging 1996;6:384–398.
29. Scheffler K. A pictorial description of steady-states in rapid magnetic resonance imaging. Concepts Magn Reson 1999;11: 291–304.
30. Haacke EM, Tkach JA. Fast MR imaging: techniques and clinical applications. AJR Am J Roentgenol 1990;155:951–964.
31. Carr HY. Steady-state free precession in nuclear magnetic resonance. Phys Rev 1958;112:1693–1701.
32. Oppelt A, Graumann R, Barfuβ H, Fischer H, Hartl W, Schajor W. FISP — a new fast MRI sequence. Electromedica 1986;54:15–18.
33. Elster AD. Gradient-echo MR imaging: techniques and acronyms. Radiology 1993;186:1–8.
34. Zur Y, Wood ML, Neuringer LJ. Spoiling of transverse magnetization in steady-state sequences. Magn Reson Med 1991;21: 251–263.
35. Denolin V, Azizieh C, Metens T. New insights into the mechanisms of signal formation in RF-spoiled gradient echo sequences. Magn Reson Med 2005;54:937–954.
36. Leupold J, Hennig J, Scheffler K. Moment and direction of the spoiler gradient for effective artifact suppression in RF-spoiled gradient echo imaging. Magn Reson Med 2008;60:119–127.
37. Duyn JH. Steady state effects in fast gradient echo magnetic resonance imaging. Magn Reson Med 1997;37:559–568.
38. Crawley AP, Wood ML, Henkelmann RM. Elimination of transverse coherences in FLASH MRI. Magn Reson Med 1988;8:248–260.
39. Prince MR. Gadolinium-enhanced MR aortography. Radiology 1994;191:155–164.
40. Wood ML, Silver M, Runge VM. Optimization of spoiler gradients in flash MRI. Magn Reson Imaging 1987;5:455–463.
41. Barkhausen J, Ruehm SG, Goyen M, Buck T, Laub G, Debatin JF. MR evaluation of ventricular function: true fast imaging with steady-state precession versus fast low-angle shot cine MR imaging: feasibility study. Radiology 2001;219:264–269.
42. Jung BA, Hennig J, Scheffler K. Single-breathhold 3D-trueFISP cine cardiac imaging. Magn Reson Med 2002;48:921–925.
43. Freeman R, Hill HDW. Phase and Intensity Anomalies in Fourier Transform NMR. J Magn Reson 1971;4:366–383.
44. Scheffler K, Heid O, Hennig J. Magnetization preparation during the steady state: fat-saturated 3D TrueFISP. Magn Reson Med 2001;45:1075–1080.
45. Atkinson DJ, Edelman RR. Cineangiography of the heart in a single breath hold with a segmented turboFLASH sequence. Radiology 1991;178:357–360.
46. Czervionke LF, Daniels DL, Wehrli FW, et al. Magnetic susceptibility artifacts in gradient-recalled echo MR imaging. AJNR Am J Neuroradiol 1988;9:1149–1155.
47. Thulborn KR, Waterton JC, Matthews PM, Radda GK. Oxygenation dependence of the transverse relaxation time of water protons in whole blood at high field. Biochim Biophys Acta 1982; 714:265–270.
48. Ogawa S, Lee TM, Kay AR, Tank DW. Brain magnetic resonance imaging with contrast dependent on blood oxygenation. Proc Natl Acad Sci U S A 1990;87:9868–9872.
49. Fazekas F, Kleinert R, Roob G, et al. Histopathologic analysis of foci of signal loss on gradient-echo T2*-weighted MR images in patients with spontaneous intracerebral hemorrhage: evidence of microangiopathy-related microbleeds. AJNR Am J Neuroradiol 1999;20:637–642.
50. Haacke EM, Xu Y, Cheng YC, Reichenbach JR. Susceptibility weighted imaging (SWI). Magn Reson Med 2004;52:612–618.
51. Rosen BR, Belliveau JW, Vevea JM, Brady TJ. Perfusion imaging with NMR contrast agents. Magn Reson Med 1990;14:249–265.
52. Ostergaard L, Weisskoff RM, Chesler DA, Gyldensted C, Rosen BR. High resolution measurement of cerebral blood flow using intravascular tracer bolus passages. Part I. Mathematical approach and statistical analysis. Magn Reson Med 1996;36: 715–725.
53. Ostergaard L, Sorensen AG, Kwong KK, Weisskoff RM, Gyldensted C, Rosen BR. High resolution measurement of cerebral blood flow using intravascular tracer bolus passages. Part II. Experimental comparison and preliminary results. Magn Reson Med 1996;36:726–736.
54. Park HW, Kim YH, Cho ZH. Fast gradient-echo chemical-shift imaging. Magn Reson Med 1988;7:340–345.
55. Reeder SB, Wen Z, Yu H, et al. Multicoil Dixon chemical species separation with an iterative least-squares estimation method. Magn Reson Med 2004;51:35–45.
56. Dixon WT. Simple proton spectroscopic imaging. Radiology 1984; 153:189–194.
57. Reeder SB, McKenzie CA, Pineda AR, et al. Water-fat separation with IDEAL gradient-echo imaging. J Magn Reson Imaging 2007; 25:644–652.
58. Siepmann DB, McGovern J, Brittain JH, Reeder SB. High-resolution 3D cartilage imaging with IDEAL SPGR at 3 T. AJR Am J Roentgenol 2007;189:1510–1515.
59. Yu H, McKenzie CA, Shimakawa A, et al. Multiecho reconstruction for simultaneous water-fat decomposition and T2* estimation. J Magn Reson Imaging 2007;26:1153–1161.
60. Wehrli FW. Time-of-flight effects in MR imaging of flow. Magn Reson Med 1990;14:187–193.
61. Sevick RJ, Tsuruda JS, Schmalbrock P. Three-dimensional time-of-flight MR angiography in the evaluation of cerebral aneurysms. J Comput Assist Tomogr 1990;14:874–881.
62. Pike GB, Hu BS, Glover GH, Enzmann DR. Magnetization transfer time-of-flight magnetic resonance angiography. Magn Reson Med 1992;25:372–379.
63. Haacke EM, Lenz GW. Improving MR image quality in the presence of motion by using rephasing gradients. AJR Am J Roentgenol 1987;148:1251–1258.
64. Mugler JP 3rd, Brookeman JR. Three-dimensional magnetization-prepared rapid gradient-echo imaging (3D MP RAGE). Magn Reson Med 1990;15:152–157.
65. Wu E, Judd RM, Vargas JD, Klocke FJ, Bonow RO, Kim RJ. Visualisation of presence, location, and transmural extent of healed Q-wave and non-Q-wave myocardial infarction. Lancet 2001;357:21–28.
66. Hawkes RC, Patz S. Rapid Fourier imaging using steady-state free precession. Magn Reson Med 1987;4:9–23.
67. Gyngell ML. The application of steady-state free precession in rapid 2DFT NMR imaging: FAST and CE-FAST sequences. Magn Reson Imaging 1988;6:415–419.
68. Moonen CT, Liu G, van Gelderen P, Sobering G. A fast gradient-recalled MRI technique with increased sensitivity to dynamic susceptibility effects. Magn Reson Med 1992;26:184–189.
69. Nayak KS, Hargreaves BA, Hu BS, Nishimura DG, Pauly JM, Meyer CH. Spiral balanced steady-state free precession cardiac imaging. Magn Reson Med 2005;53:1468–1473.
70. King KF, Foo TK, Crawford CR. Optimized gradient waveforms for spiral scanning. Magn Reson Med 1995;34:156–160.
71. Glover GH, Lai S. Self-navigated spiral fMRI: interleaved versus single-shot. Magn Reson Med 1998;39:361–368.
72. Mansfield P. Multi planar image formation using NMR spin echoes. J Phys C 1977;10:L55–L58.
73. Schmitt F, Stehling M, Turner R. Echo planar imaging: theory, technique and application. New York: Springer; 1998.
74. Tsao J. Ultrafast imaging: principles, pitfalls, solutions, and applications. J Magn Reson Imaging 2010;32:252–266.